Journal of Hazardous Materials 186 (2011) 590–601

Contents lists available at ScienceDirect

Journal of Hazardous Materials

journal homepage: www.elsevier.com/locate/jhazmat

# Study of arsenopyrite weathering products in mine wastes from abandoned tungsten and tin exploitations

A. Murciego[a], E. Álvarez-Ayuso[b,*], E. Pellitero[a], Mª A. Rodríguez[c], A. García-Sánchez[b], A. Tamayo[d], J. Rubio[d], F. Rubio[d], J. Rubin[e]

[a] Department of Geology, Plza. de los Caídos s/n. Salamanca University, 37008 Salamanca, Spain
[b] Department of Environmental Geochemistry, IRNASA (CSIC), Apdo. 257, 37071 Salamanca, Spain
[c] Faculty of Sciences, Crystallography and Mineralogy Area, Avd. Elvas s/n. Extremadura University, 06071 Badajoz, Spain
[d] Ceramic and Glass Institute (CSIC), c/Kelsen, 5, 28049 Cantoblanco, Madrid, Spain
[e] Material Science Institute of Aragón, CSIC-Zaragoza University, c/María de Luna 3, 50009 Zaragoza, Spain

ARTICLE INFO

*Article history:*
Received 30 July 2010
Received in revised form 5 November 2010
Accepted 9 November 2010
Available online 13 November 2010

*Keywords:*
Arsenopyrite
Arsenic
Mine wastes
Secondary or weathering products
Environmental risk assessment

ABSTRACT

Arsenopyrite-rich wastes from abandoned tungsten and tin exploitations were studied to determine the composition and characteristics of the secondary phases formed under natural weathering conditions so as to assess their potential environmental risk. Representative weathered arsenopyrite-bearing rock wastes collected from the mine dumps were analysed using the following techniques: X-ray powder diffraction (XRD) analysis, polarizing microscopy analysis, electron microprobe analysis (EMPA) and microRaman and Mössbauer spectroscopies. Scorodite, pharmacosiderite and amorphous ferric arsenates (AFA) with Fe/As molar ratios in the range 1.2–2.5 were identified as secondary arsenic products. The former showed to be the most abundant and present in the different studied mining areas. Its chemical composition showed to vary in function of the original surrounding rock mineralogy in such a way that phosphoscorodite was found as the mineral variety present in apatite-containing geoenvirons. Other ever-present weathering phases were goethite and hydrous ferric oxides (HFO), displaying, respectively, As retained amounts about 1 and 20% (expressed as $As_2O_5$). The low solubility of scorodite, the relatively low content of AFA and the formation of compounds of variable charge, mostly of amorphous nature, with high capacity to adsorb As attenuate importantly the dispersion of this element into the environment from these arsenopyrite-bearing wastes.



## 1. Introduction

Arsenic is currently regarded as one of the most toxic inorganic pollutants, being responsible for severe environmental and health impacts. Contamination with As is a global concern due to its worldwide distribution. In nature As occurs as a constituent of different minerals, but its release has been promoted by anthropogenic activities such as mining. More than 300 As minerals are known, with approximately 60% being arsenates, 20% sulphides and sulphosalts and the remaining 20% including arsenides, arsenites, oxides and elemental As [1,2]. Sulphide deposits are the main mineral source of As, in which this element can be present in high concentrations. Particularly, arsenopyrite (FeAsS) is the most common As-bearing mineral, being found in a range of ore deposits. Thus, arsenopyrite is the ubiquitous As-bearing mineral in a variety of hydrothermal environments, from high-temperature magmatic-hydrothermal porphyry-style Sn–W and Cu(±Au) deposits to mesothermal polymetallic Cu–Pb–Zn–Ag and gold deposits [3]. These deposits have been extensively exploited for the economic ore minerals, inducing a wide legacy of As in mine spoils.

Arsenopyrite is stable under reducing conditions, and mine tailings containing arsenopyrite should be chemically stable during long-term storage provided they are kept water-saturated and moderately reduced [4]. Conversely, under oxidising conditions the mobilisation and migration of As into the environment can take place. All over the world, there are many historic derelict mines that have generated a large amount of arsenopyrite-bearing waste rocks and tailings. These wastes have been poorly managed, allowing oxidation processes to occur. Arsenopyrite can be easily oxidised by both $O_2$ and $Fe^{3+}$, this process being promoted by micro-organisms, especially by acidophilic Fe- and S-oxidising bacteria [5].

Secondary As compounds such as scorodite ($FeAsO_4{\cdot}2H_2O$), pharmacosiderite ($KFe_4(AsO_4)_3(OH)_4{\cdot}6\text{-}7H_2O$), arsenolite ($As_2O_3$), arseniosiderite ($Ca_2Fe_3(AsO_4)_3O_2{\cdot}3H_2O$) and amorphous ferric arsenate-(sulphate) have been reported as the most common prod-

* Corresponding author. Tel.: +34 923219606; fax: +34 923219609.
*E-mail address:* esther.alvarez@irnasa.csic.es (E. Álvarez-Ayuso).

0304-3894/$ – see front matter © 2010 Elsevier B.V. All rights reserved.
doi:10.1016/j.jhazmat.2010.11.033

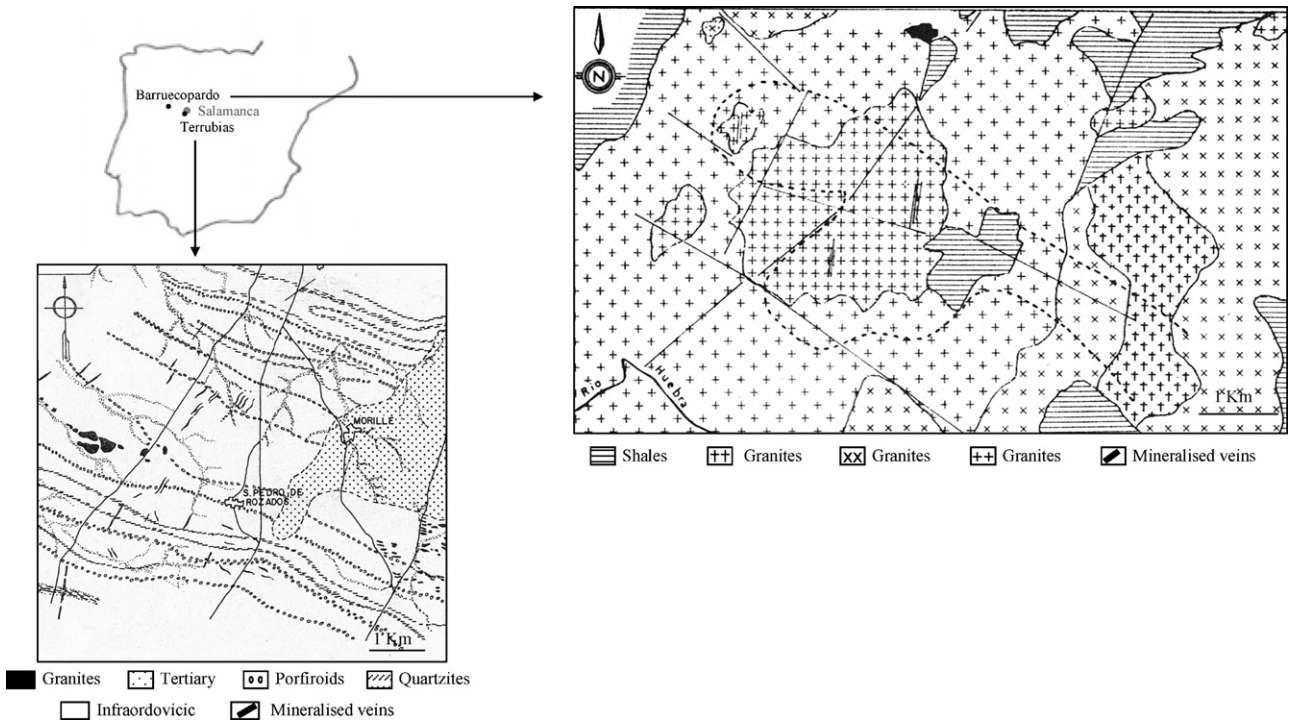


**Fig. 1.** Localisation of the Barruecopardo and Terrubias mines and geologic outcrops in these areas.

ucts of arsenopyrite weathering in natural environments, together with other secondary compounds such as goethite (FeO(OH)), ferrihydrite ($Fe_2O_3{\cdot}0.5H_2O$) or amorphous hydrous ferric oxides (HFO) [6–11]. The genesis of these secondary products is dependent on the original ore mineralogy and on the processes that have occurred during their formation (mainly redox and pH changes) [2]. The release of As from mine wastes is controlled by precipitation–dissolution and adsorption–desorption reactions involving the secondary compounds generated during the weathering of arsenopyrite [12]. Therefore, their identification and characterisation are crucial for the risk assessment and environmental control of the historic arsenopyrite-bearing mine spoils. Whereas many works studying wastes from gold mining areas have been performed [4,7,8,11,13–17], only some efforts have been devoted to study wastes from tungsten- and tin-mining districts [18–20].

The aim of this work is to study the mine wastes from abandoned tungsten and tin exploitations in order to identify and characterise the secondary products generated from arsenopyrite weathering and to assess the potential environmental risk of such wastes.

## 2. Materials and methods

### 2.1. Study areas

Two abandoned mine exploitations were considered in this study, the Barruecopardo and Terrubias mines, located, respectively, in the north-west and centre of the Salamanca province, Spain (Fig. 1). The Barruecopardo mine corresponds to the most important tungsten deposit in Spain, exploited extensively from 1912 to 1983. This is constituted by subvertical quartz veins disposed in parallel intragranitic bands. The main minerals present are scheelite ($CaWO_4$) and wolframite ($(Fe,Mn)WO_4$), which constitute the ore, and arsenopyrite, pyrite ($FeS_2$), chalcopyrite ($CuFeS_2$) and ilmenite ($FeTiO_3$) as primary minerals. These minerals appear in the veins and on the borders of granite in which apatite ($Ca_{10}(PO_4)_6(OH,F,Cl,Br)_2$) appears as an accessory mineral [21]. The Terrubias mine corresponds to a tungsten- and tin-rich deposit worked intermittently during the last century, and whose exploitation ceased more than three decades ago. Two Sn–W mineralisation types are present in this mining area: stratiform, in calcosilicate bands, and in subvertical veins of NNE-NE and N100-130E directions, cutting the scheelite-rich calcosilicate bands. The paragenesis of these veins is dominated by quartz, mica, tourmaline, wolframite, scheelite, cassiterite ($SnO_2$) and arsenopyrite [22].

### 2.2. Characterisation of weathered arsenopyrite-bearing wastes

About 25 samples of weathered arsenopyrite were collected from the Barruecopardo and Terrubias mining areas. All these samples were surface samples. In the studied mining areas wastes were dispersed on surface or accumulated in very small dumps where the existence of weathering profiles was not observed. The weathering products show yellow-greenish colours, graduating towards orange-reddish tonalities in the sample borders, where these display numerous holes (Figs. 2a and 3a). Such weathered arsenopyrite samples were studied by X-ray powder diffraction (XRD) analysis, polarizing microscopy analysis, electron microprobe analysis (EMPA) and microRaman and Mössbauer spectroscopies. X-ray diffraction analyses were performed on a D8 Advance Bruker diffractometer equipped with a diffracted-beam graphite monochromator, using the $CuK_\alpha$ radiation ($\lambda K_\alpha = 1.54$ Å). Solids were scanned as unoriented powder samples from 4° to 60° $2\theta$ with a 0.04 $2\theta$ step and a 1 s per step counting time. The analyses by polarizing microscopy were carried out on polished thin sections using a Leica DMLP microscope in both transmitted and reflected light. Electron microprobe analyses for chemical analyses and for electron backscatter images were conducted on carbon-coated polished thin sections in wavelength-dispersive mode using a JEOL Superprobe JXA-8900M electron probe microanalyser. The analysed elements were Al, Mn, P, Ba, As, Si, Fe, S, K, Cu, Pb, Ca and Zn. Operating conditions were an accelerating voltage of 15 kV and a beam current of 2 nA with a spot size of 1–5 μm and spot

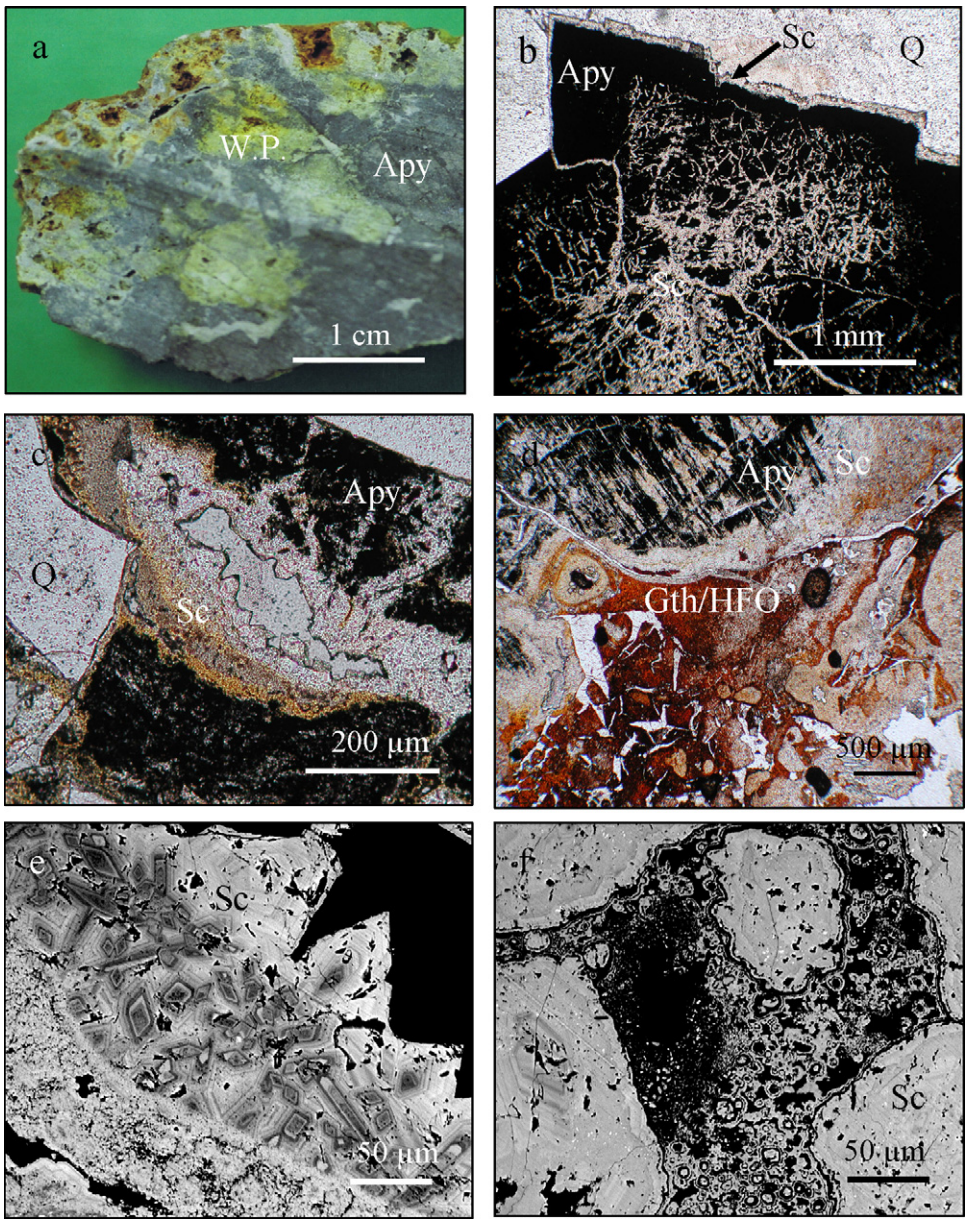


**Fig. 2.** Images of the arsenopyrite weathering products from Barruecopardo mine wastes: (a) Hand sample of arsenopyrite, (b) Microscopic image in polarizing transmitted light of scorodite on the borders, in veins and inside of arsenopyrite, (c) Microscopic image in polarizing transmitted light of scorodite crystals, (d) Microscopic image in polarizing transmitted light of red-blackish phases occurring on the borders of scorodite, (e) Electron backscatter image of zoned crystals of scorodite, showing intensified grey tonalities towards the crystal cores (detail of c) and (f) Electron backscatter image of colloform scorodite with zonation, showing intensified grey tonalities towards the cores (WP: weathering products, Sc: scorodite, Apy: arsenopyrite, Gth: goethite and Q: quartz).

analysis and background collection times of 10 and 5 s, respectively. Calibration was carried out using the following standards: sillimanite for Al, almandine for Fe, pyrolusite for Mn, apatite for P, witherite for Ba, gallium arsenide for As, albite for Si, galena for S and Pb, microcline for K, chalcopyrite for Cu, kaersutite for Ca and gahnite for Zn. The microRaman spectra of polished thin sections of samples were recorded with a Via Renishaw spectrometer equipped with a Charge Coupled Device (CCD) detector. Samples were excited with a 784 nm laser operating at 25 mW. A 50× objective lens was employed to focus the laser beam. The overall spectral resolution was 2 $cm^{-1}$. The Mössbauer spectra of powder samples were recorded at room temperature in transmission mode on a constant acceleration Mössbauer spectrometer equipped with a $^{57}$Co-Rh matrix source. α-Fe foil was used for velocity calibration. Spectra were fitted using the Mössbauer fitting program NORMOS written by R.A. Brand.

### *2.3. Environmental risk assessment of the arsenopyrite-bearing mine wastes*

In order to more accurately assess the environmental risks that may entail the mine wastes present in the Barruecopardo and Terrubias mining areas, these wastes were subjected to the subsequent determinations: pH, net neutralisation potential (NNP), toxicity and bioavailable content of As and other toxic elements (Cu, Pb, Zn and Cd). pH was analysed potentiometrically in a paste saturated with water. NNP was evaluated following the method of Sobek et al. [23] as a measure of the difference between the neutralising potential (NP) and the acid potential (AP). Accordingly, AP was derived by calculating the theoretical quantity of acid that could be produced if the total S content of wastes is converted to sulphuric acid, and expressing this quantity in kg of $CaCO_3$ required to neutralise the acidity produced from 1 t of waste material (AP

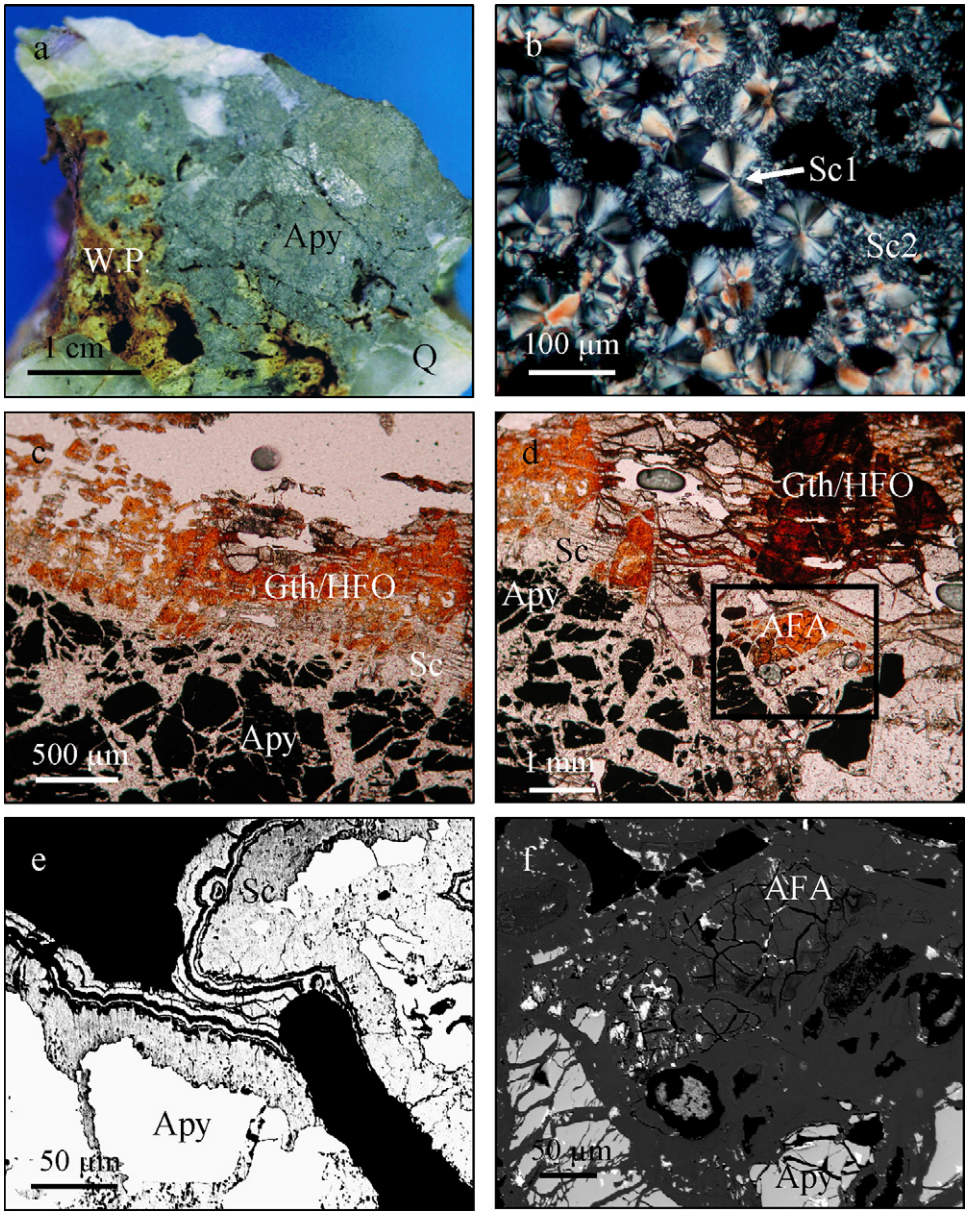


**Fig. 3.** Images of the arsenopyrite weathering products from Terrubias mine wastes: (a) Hand sample of arsenopyrite, (b) Microscopic image in polarizing transmitted light of sferulitic scorodite (Sc1) and microcrystalline massive scorodite (Sc2), (c) Microscopic image in polarizing transmitted light of weathering products of arsenopyrite (scorodite, goethite and HFO), (d) Microscopic image in polarizing transmitted light of weathering products of arsenopyrite, showing orange-reddish phases corresponding to AFA, (e) Electron backscatter image of colloform scorodite and (f) Electron backscatter image of AFA (detail of d) (WP: weathering products, Sc: scorodite, Apy: arsenopyrite, Gth: goethite and Q: quartz).

(kg $CaCO_3$ $t^{-1}$) = 31.25 wt.% S), and NP was determined by neutralising finely ground waste samples with 0.1 M HCl at 90 °C, and expressing the corresponding results in kg $CaCO_3$ $t^{-1}$. Toxicity was established according to the TCLP test method. Thus, waste samples underwent an agitation period of 18 h with buffered acetic acid (pH 4.93 ± 0.05) on a vertical rotary shaker (30 rpm), using a liquid/solid (L/S) ratio of 20 L $kg^{-1}$. The bioavailable content of As was extracted according to the method of Wenzel et al. [24] by subjecting waste samples to an agitation period of 16 h with 0.05 M $(NH_4)_2SO_4$, using a L/S ratio of 25 L $kg^{-1}$. The bioavailable content of the other toxic elements (occurring as cationic species) was determined following an EDTA extraction procedure [25] in which waste samples underwent an agitation period of 1 h with 1 M $CH_3COONH_4$ + 0.02 M EDTA, employing a L/S ratio of 10 L $kg^{-1}$. The extracts resulting from these three extraction processes were analysed for As and/or Cu, Pb, Zn and Cd by inductively coupled plasma-atomic emission spectrometry (ICP-AES) using a Varian 720-ES unit.

Additionally, in order to obtain more information on the environmental impact of these mine wastes the water quality of the nearby ponds was also evaluated, determining their pH, Eh and concentrations of sulphate, As and other toxic elements (Cu, Pb, Zn and Cd). The concentrations of such species were analysed by ICP-AES.

## 3. Results and discussion

### *3.1. Characterisation of weathered arsenopyrite-bearing wastes from the Barruecopardo mine*

#### *3.1.1. X-ray diffraction analyses*

XRD analyses were performed on the bulk samples collected from the Barruecopardo mine waste rock dumps and on the yellow-

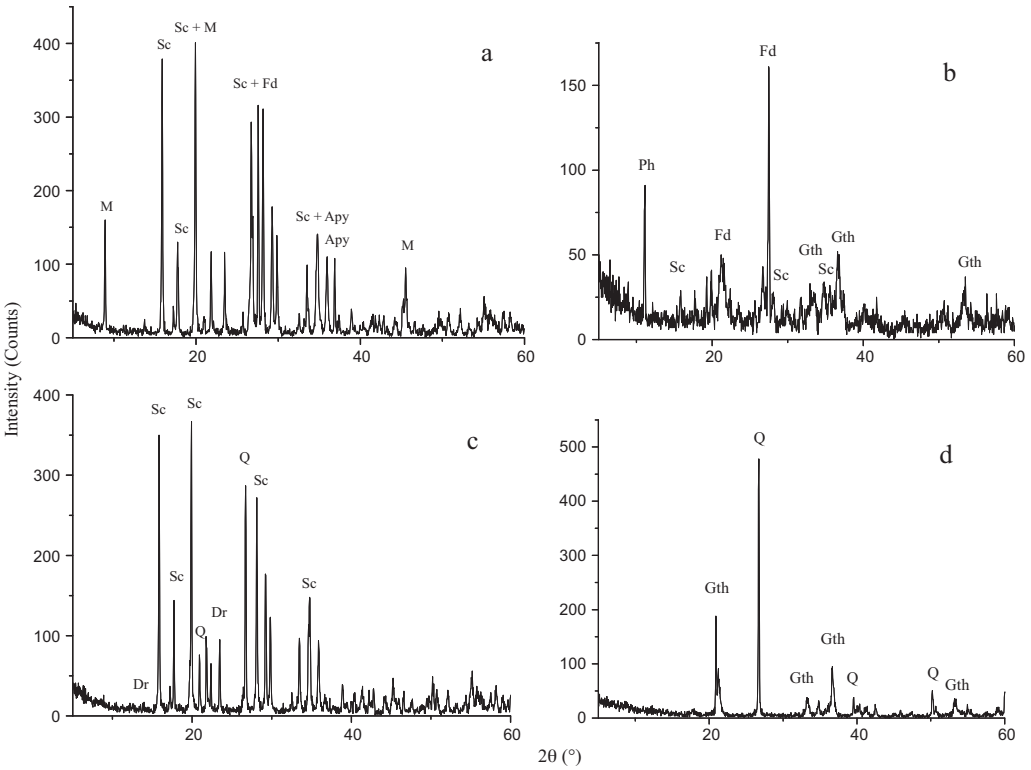


**Fig. 4.** XRD patterns of the yellow-greenish and orange-reddish phases occurring on the weathered waste rocks from the Barruecopardo and Terrubias mines (a: yellow-greenish phases (Barruecopardo), b: orange-reddish phases (Barruecopardo), c: yellow-greenish phases (Terrubias) and d: orange-reddish phases (Terrubias); M: muscovite, Sc: scorodite, Fd: K-feldspar, Apy: arsenopyrite, Ph: pharmacosiderite, Gth: goethite, Dr: dravite and Q: quartz).

greenish and orange-reddish phases distinguished on them. Bulk samples showed scorodite, pharmacosiderite and goethite as secondary minerals, and the presence of primary minerals such as quartz, muscovite, K-feldspar and arsenopyrite, which are known constituents of the ore gangue and surrounding rocks. The XRD analyses carried out specifically on the yellow-greenish phases revealed that these are mainly composed of scorodite; the presence of the primary minerals muscovite, K-feldspar and arsenopyrite was also detected (Fig. 4a). Pharmacosiderite and goethite were found as the main secondary minerals composing the orange-reddish phases, with scorodite only present in minor amounts; the presence of the primary mineral K-feldspar was also detected (Fig. 4b).

### 3.1.2. Polarizing microscopy analysis

Microscopically different modes of occurrence of arsenopyrite can be distinguished. Thus, arsenopyrite appears as unweathered idiomorphic crystals, in slightly weathered crystals and in highly to completely weathered crystals, mostly keeping their original morphology. Two kinds of arsenopyrite weathering products are observed: scorodite and red-blackish phases. Scorodite is the most abundant oxidation product. This occurs on the arsenopyrite crystal borders, along small cracks, inside of arsenopyrite (Fig. 2b) and following the crystallographic planes. On occasions scorodite completely replaces arsenopyrite crystals, pseudomorphing them. More usual is the presence of corroded relicts of arsenopyrite inside scorodite. This mineral is present in different textures: microcrystalline massive, spherulitic and colloform, and in prismatic crystals of varying sizes (from μm to tens of μm) (Fig. 2c). The red-blackish phases occur bordering the scorodite. These could correspond to HFO and goethite (Fig. 2d), but no clear identification of them could be established due to the product mixture and to the low crystallinity and relatively low content of goethite, as reflected by the corresponding XRD pattern.

### 3.1.3. Electron microprobe analysis

A total of 95 chemical analyses were performed by EMPA on the observed arsenopyrite weathering products (scorodite (80) and red-blackish phases (15)). The specific number of analyses performed on each weathering phase is representative of the phase abundance. These analyses are indicated in Table 1 (only analyses given element contents for single phases were reflected, whereas those indicating phase mixture or presence of arsenopyrite were omitted). According to these analyses, the main general differential characteristics of scorodite are: relatively high P contents (from 0.26 to 9.01% $P_2O_5$), moderately low contents of S (up to 1.49% $SO_3$) and minor or trace concentrations of other elements (Al, Si and Cu). This scorodite displays Fe/As molar ratios in the range 1.04–1.47, differing from the scorodite theoretical value (Fe/As = 1). The frequency distribution is as follows: 13% (Fe/As = 1–1.1), 41% (Fe/As = >1.1–1.2), 31% (Fe/As = >1.2–1.3) and 15% (Fe/As = >1.3). Therefore, an important proportion of the analyses performed on scorodite (>85%) shows Fe/As molar ratios increased in more than 10% compared to the ideal value. This As deficiency is explained by the corresponding P enrichment shown by this mineral, giving Fe/(As + P) molar ratios in the range 0.92–1.26. The frequency distribution is as follows: 80% (Fe/(As + P) = >0.9–1.1), 16% (Fe/(As + P) = >1.1–1.2) and 4% (Fe/(As + P) = >1.2). Hence, most of the analyses performed on scorodite agrees well with the proposed elemental constitution. This compositional characteristic denotes that this mineral is an intermediate term between scorodite and strengite ($FePO_4{\cdot}2H_2O$), corresponding to P-rich scorodite or phosphoscorodite ($Fe(As,P)O_4{\cdot}2H_2O$). P exists in scorodite by isomorphous substitution of $PO_4^{3-}$ for $AsO_4^{3-}$ or by simultaneous incorporation into the crystal lattice, and is mineralogically expressed as a solid solution of scorodite and strengite, though they form only a partial solid-solution series. No continuous solid solution is produced due to the size difference between $AsO_4^{3-}$ and $PO_4^{3-}$ [26]. The electron backscatter images also suggest such

**Table 1**
Chemical analyses of the arsenopyrite weathering products in the Barruecopardo mine wastes ($Sc_{ms}$, $Sc_{sf}$, $Sc_{cl}$ and $Sc_{cry}$: scorodite microcrystalline massive, spherulitic, colloform and in crystals, and R-b ph: Red-blackish phases).

| Phases | $Fe_2O_3$ (%) | $As_2O_5$ (%) | $P_2O_5$ (%) | $SO_3$ (%) | $Al_2O_5$ (%) | $SiO_2$ (%) | CuO (%) |
|---|---|---|---|---|---|---|---|
| $Sc_{ms}$ | 35.0 | 44.9 | 4.16 | n.d. | 2.21 | n.d. | n.d. |
| $Sc_{ms}$ | 34.9 | 45.0 | 4.34 | n.d. | 2.53 | n.d. | n.d. |
| $Sc_{ms}$ | 35.3 | 43.4 | 4.24 | n.d. | 2.14 | n.d. | n.d. |
| $Sc_{ms}$ | 35.6 | 48.1 | 0.26 | 0.76 | 0.17 | n.d. | n.d. |
| $Sc_{ms}$ | 35.5 | 48.2 | 0.27 | 0.61 | 0.53 | n.d. | n.d. |
| $Sc_{ms}$ | 36.1 | 49.5 | 0.36 | 0.42 | 0.84 | n.d. | n.d. |
| $Sc_{ms}$ | 35.0 | 48.3 | 0.33 | 0.32 | 0.94 | n.d. | n.d. |
| $Sc_{ms}$ | 36.6 | 47.0 | 1.33 | 1.15 | n.d. | n.d. | n.d. |
| $Sc_{ms}$ | 34.8 | 43.2 | 2.20 | 0.12 | 0.27 | 0.73 | n.d. |
| $Sc_{ms}$ | 35.3 | 45.9 | 1.59 | 0.48 | 0.10 | 0.23 | n.d. |
| $Sc_{ms}$ | 37.4 | 43.3 | 5.35 | n.d. | n.d. | n.d. | n.d. |
| $Sc_{ms}$ | 37.3 | 42.8 | 3.53 | 0.87 | n.d. | n.d. | n.d. |
| $Sc_{ms}$ | 37.3 | 42.9 | 4.25 | 0.38 | n.d. | n.d. | n.d. |
| $Sc_{ms}$ | 35.9 | 48.0 | 1.37 | 0.75 | n.d. | n.d. | n.d. |
| $Sc_{ms}$ | 36.8 | 40.5 | 6.32 | 0.45 | n.d. | n.d. | n.d. |
| $Sc_{ms}$ | 37.4 | 43.4 | 5.28 | n.d. | n.d. | n.d. | n.d. |
| $Sc_{ms}$ | 37.9 | 41.4 | 6.73 | n.d. | n.d. | n.d. | n.d. |
| $Sc_{ms}$ | 33.1 | 39.2 | 8.02 | n.d. | 0.40 | n.d. | n.d. |
| $Sc_{ms}$ | 35.0 | 47.0 | 0.88 | 1.25 | n.d. | n.d. | n.d. |
| $Sc_{ms}$ | 35.5 | 46.8 | 0.90 | 1.02 | n.d. | n.d. | n.d. |
| $Sc_{ms}$ | 36.6 | 42.2 | 5.33 | n.d. | n.d. | n.d. | n.d. |
| $Sc_{ms}$ | 37.4 | 42.8 | 5.64 | n.d. | n.d. | n.d. | n.d. |
| $Sc_{sf}$ | 37.2 | 46.5 | 1.26 | 0.86 | n.d. | n.d. | n.d. |
| $Sc_{sf}$ | 37.1 | 46.1 | 1.13 | 0.91 | n.d. | n.d. | n.d. |
| $Sc_{sf}$ | 36.3 | 45.0 | 0.96 | 1.05 | 0.18 | n.d. | n.d. |
| $Sc_{sf}$ | 36.5 | 45.6 | 1.82 | 0.99 | 0.45 | 0.50 | n.d. |
| $Sc_{sf}$ | 35.2 | 45.7 | 0.85 | 0.79 | 1.17 | 1.17 | n.d. |
| $Sc_{cl}$ | 37.0 | 46.8 | 2.08 | n.d. | 0.16 | n.d. | n.d. |
| $Sc_{cl}$ | 37.1 | 45.7 | 1.44 | 0.90 | 0.33 | n.d. | n.d. |
| $Sc_{cl}$ | 37.5 | 45.7 | 2.02 | 0.51 | 0.20 | n.d. | n.d. |
| $Sc_{cl}$ | 36.9 | 47.8 | 0.93 | n.d. | 0.37 | n.d. | n.d. |
| $Sc_{cl}$ | 37.0 | 46.4 | 2.07 | 0.26 | 0.27 | n.d. | n.d. |
| $Sc_{cl}$ | 37.7 | 43.9 | 4.74 | 0.01 | 0.24 | n.d. | n.d. |
| $Sc_{cl}$ | 37.2 | 44.9 | 1.60 | 1.09 | 0.18 | n.d. | n.d. |
| $Sc_{cl}$ | 36.5 | 46.9 | 0.75 | 0.96 | n.d. | n.d. | n.d. |
| $Sc_{cl}$ | 36.7 | 45.2 | 1.87 | 1.29 | 0.16 | n.d. | 0.56 |
| $Sc_{cl}$ | 38.2 | 40.7 | 6.36 | 1.49 | 0.44 | n.d. | n.d. |
| $Sc_{cl}$ | 39.2 | 42.8 | 1.17 | 0.74 | 0.34 | n.d. | n.d. |
| $Sc_{cl}$ | 37.8 | 44.4 | 1.52 | 1.03 | 0.21 | n.d. | n.d. |
| $Sc_{cry}$ | 38.8 | 46.8 | 1.42 | n.d. | 0.14 | n.d. | n.d. |
| $Sc_{cry}$ | 39.0 | 47.3 | 2.29 | n.d. | 0.20 | n.d. | n.d. |
| $Sc_{cry}$ | 39.0 | 40.9 | 8.84 | n.d. | 0.13 | n.d. | n.d. |
| $Sc_{cry}$ | 37.8 | 42.5 | 7.92 | n.d. | 2.22 | n.d. | n.d. |
| $Sc_{cry}$ | 39.2 | 45.1 | 5.54 | n.d. | 0.91 | n.d. | n.d. |
| $Sc_{cry}$ | 37.4 | 43.0 | 7.02 | n.d. | 3.08 | 1.10 | n.d. |
| $Sc_{cry}$ | 39.2 | 45.0 | 7.06 | n.d. | 0.66 | n.d. | n.d. |
| $Sc_{cry}$ | 41.7 | 40.7 | 9.01 | n.d. | 0.42 | 0.26 | n.d. |
| $Sc_{cry}$ | 39.8 | 46.6 | 2.87 | n.d. | 0.69 | n.d. | n.d. |
| $Sc_{cry}$ | 37.4 | 47.4 | 4.59 | n.d. | 2.15 | n.d. | n.d. |
| $Sc_{cry}$ | 36.1 | 41.8 | 7.77 | n.d. | 2.57 | 0.12 | n.d. |
| R-b ph | 57.3 | 5.66 | 0.30 | n.d. | 1.86 | n.d. | n.d. |
| R-b ph | 55.8 | 5.93 | 0.34 | n.d. | 1.89 | n.d. | n.d. |
| R-b ph | 61.3 | 6.10 | 0.37 | n.d. | 2.26 | n.d. | n.d. |
| R-b ph | 57.1 | 11.9 | 0.78 | 0.24 | n.d. | n.d. | n.d. |
| R-b ph | 62.3 | 6.66 | 0.63 | 0.68 | n.d. | n.d. | n.d. |
| R-b ph | 65.6 | 6.89 | 0.71 | 0.78 | n.d. | n.d. | n.d. |

elemental composition. Thus, concentric zonation is observed in scorodite crystals (Fig. 2e), showing P enrichment from the borders to the core (with $P_2O_5$ values from 1.42 to 9.01%). Accordingly, grey tonalities are intensified towards the crystal cores as elements with low atomic number (P) appear darker than those with high atomic number (As). Zonation is also observed in the colloform scorodite (Fig. 2f), with $P_2O_5$ contents varying from 0.75 to 6.36%. The P enrichment shown by the scorodite developed in this mining area should be related to the occurrence of apatite in the surrounding rocks of the exploited ore deposit.

The analyses performed on the red-blackish phases show $Fe_2O_3$ and $As_2O_5$ contents comprised, respectively, in the ranges 55.8–65.6% and 5.66–11.9%. Such values suggest that these phases are not composed of single goethite as their $Fe_2O_3$ content should be higher (theoretically close to 80%) and their $As_2O_5$ concentration should display much lower values. Different studies performed on the As(V) adsorption capacity of goethite [27,28] have revealed that the maximum As(V) adsorption values attained by this mineral are about 1% $As_2O_5$. Conversely, HFO display much elevated As(V) adsorption capacities due to their higher number of reactive hydroxyl groups [27,29]. The relatively high $As_2O_5$ contents shown by these phases together with their apparent hydrous character (as derived from the low total elemental composition) suggest the presence of HFO as important constituents of them. It is also worth mentioning that the $P_2O_5$ content of these weathering phases ranges from 0.30 to 0.78%. It is well known the ability of compounds of variable charge, as those present in such phases, to adsorb phosphate. This ability and the presence of apatite in the studied area

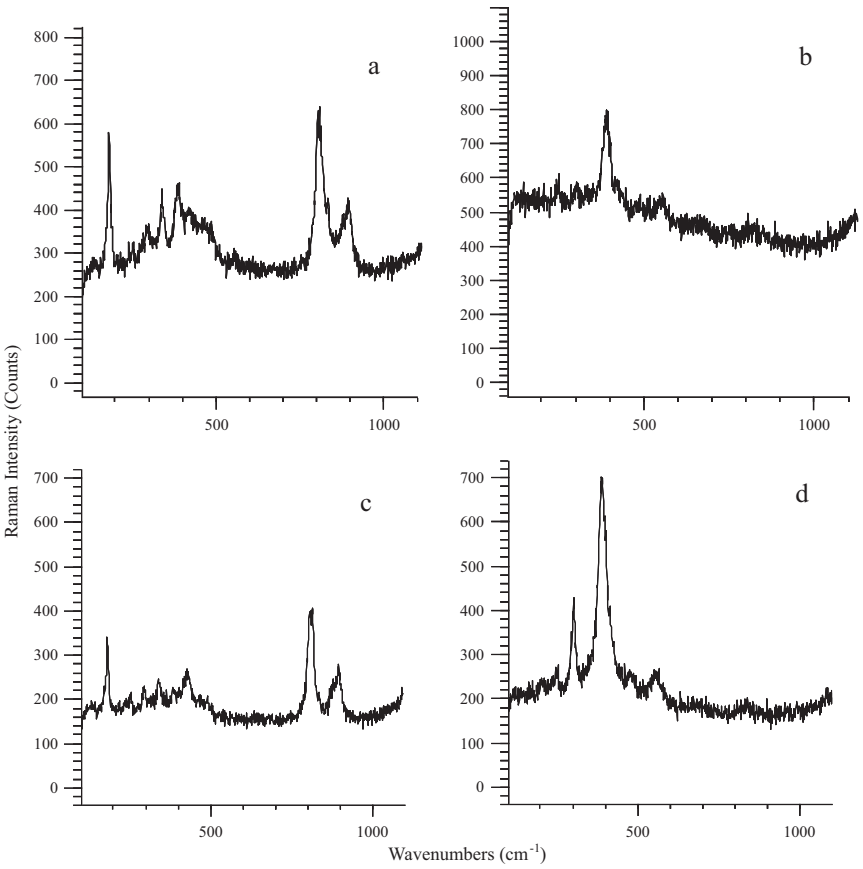


**Fig. 5.** Representative microRaman spectra of the arsenopyrite weathering products in the Barruecopardo and Terrubias mine wastes (a: scorodite (Barruecopardo), b: goethite (Barruecopardo), c: scorodite (Terrubias) and d: goethite (Terrubias)).

explain such $P_2O_5$ contents. Phosphate and arsenate are chemical analogues with comparable dissociation constants for their acids and similar chemical properties, competing directly for binding sites. Moreover, at similar concentrations phosphate outcompetes arsenate for adsorption sites because of its smaller size and higher charge density [30].

### 3.1.4. MicroRaman spectroscopy

The microRaman spectra of the weathering phase identified as scorodite agree well with that of scorodite reported in literature [31–33], confirming the important occurrence of this mineral as a secondary product of arsenopyrite. The representative microRaman spectrum corresponding to the most crystalline scorodite (Fig. 5a) displays in the arsenate stretching region two high intensity bands at 812 $cm^{-1}$ ($\nu_1$, symmetric stretching mode) and at 892 $cm^{-1}$ ($\nu_3$, asymmetric stretching mode), characteristic of scorodite. The low wavelength region is characterised by several bands at 338 and 388 $cm^{-1}$ ($\nu_2$, symmetric bending mode) and at 419, 458 and 485 $cm^{-1}$ (asymmetric bending mode), also in accordance to the low wavelength region of scorodite. The microRaman spectra derived from zoned crystals of scorodite with different P concentrations do not reflect such compositional variations. Also similar vibrational positions are shown by the microRaman spectra corresponding to scorodite in microcrystalline forms, although exhibiting poor definition.

The microRaman spectra corresponding to the red-blackish phases distinguished by polarizing microscopy show goethite as the only crystalline secondary mineral occurring in them. Its representative microRaman spectrum is displayed in Fig. 5b, where the following bands are distinguishable: 249, 303, 390, 485 and 556 $cm^{-1}$. These bands are in good agreement with the characteristic pure goethite Raman modes reported by de Faria et al. [34]. Several microanalyses performed on these red-blackish phases give spectra with no apparent Raman modes, indicating the amorphous nature of some of their constituents, which could be compatible with the presence of HFO.

### 3.1.5. Mössbauer spectroscopy

The Mössbauer analyses were performed on the yellow-greenish and orange-reddish phases distinguished on the waste rocks collected from the mine dumps. The representative Mössbauer spectra obtained from the analyses of these phases are shown in Fig. 6a and b, respectively. According to Takano et al. [35], scorodite has values of $\delta = 0.39$ mm $s^{-1}$ and QS = 0.42 mm $s^{-1}$, whereas pharmacosiderite displays values of $\delta = 0.36$ mm $s^{-1}$ and QS = 0.68 mm $s^{-1}$. The spectrum corresponding to the yellow-greenish phases is solved assuming a single doublet fit. Its Mössbauer parameters are $\delta = 0.39$ mm $s^{-1}$ and QS = 0.44 mm $s^{-1}$, which are in agreement with those of scorodite. The spectrum corresponding to the orange-reddish phases is principally a doublet accompanied by a weaker sextet. The Mössbauer parameters of the main component are $\delta = 0.37$ mm $s^{-1}$ and QS = 0.57 mm $s^{-1}$. The doublet has values intermediate between those of scorodite and pharmacosiderite, suggesting the presence of both minerals in these phases. The sextet is related to goethite with $B_{HF} = 34$T. This value is significantly reduced when compared with the typical $B_{HF}$ value of goethite, which is 38T [36]. Structural defects, like vacancies and/or isomorphic substitution, and also small particle size are the main contributors to reduced $B_{HF}$ values [37].

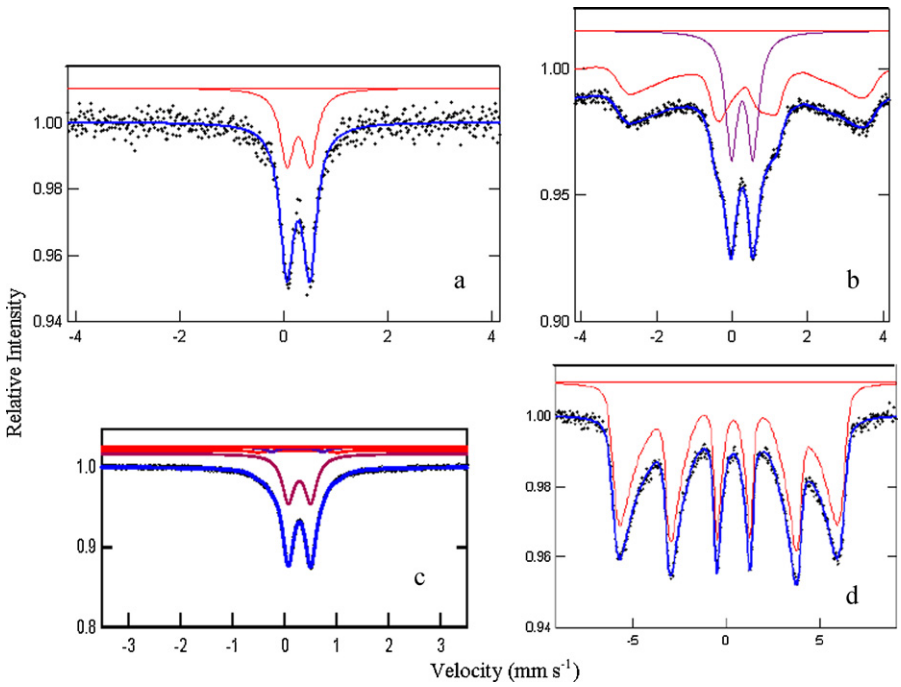


**Fig. 6.** Representative Mössbauer spectra of the yellow-greenish (a and c) and orange-reddish phases (b and d) occurring on the weathered waste rocks from the Barruecopardo and Terrubias mines (a: scorodite (Barruecopardo), b: scorodite + pharmacosiderite and goethite (Barruecopardo), c: scorodite (Terrubias) and d: goethite (Terrubias)).

### *3.2. Characterisation of weathered arsenopyrite-bearing wastes from the Terrubias mine*

#### *3.2.1. X-ray diffraction analyses*

XRD analyses performed on the bulk samples collected from the Terrubias mine waste rock dumps showed scorodite and goethite as secondary minerals, and the presence of the primary minerals quartz, dravite (a tourmaline variety) and arsenopyrite. Similar mineralogical composition, except for the presence of goethite, was displayed by the XRD analyses performed on the yellow-greenish phases occurring on the weathered waste rock samples (Fig. 4c), whereas goethite was the only crystalline secondary mineral detected in the orange-reddish phases together with quartz as primary mineral (Fig. 4d).

#### *3.2.2. Polarizing microscopy analysis*

Microscopically arsenopyrite appears as unweathered euhedral crystals embedded in quartz, as partial or totally weathered crystals that keep their original shape and in relicts with corroded borders. Several arsenopyrite weathering products are distinguished: scorodite, goethite, red-blackish phases and orange-reddish phases. Scorodite is the most abundant oxidation product. This mineral is present in different textures: microcrystalline massive, spherulitic and colloform. The latter is very profuse, whereas the spherulitic texture is mainly limited to zones of high porosity. The massive texture is also widespread, appearing around the arsenopyrite, filling small cracks in quartz and locally aggregating the scorodite spherulites (Fig. 3b). Goethite and the other red-blackish phases occur bordering the scorodite (Fig. 3c). These latter phases are isotropes, with numerous internal reflections. Such secondary products seem to correspond to HFO. The orange-reddish phases are very rare and generally occur embedded in scorodite masses and, more rarely, in direct contact with corroded relicts of arsenopyrite. These show a cracked appearance (Fig. 3d), being consistent with amorphous ferric arsenates (AFA).

#### *3.2.3. Electron microprobe analysis*

A total of 115 chemical analyses were performed by EMPA on the observed arsenopyrite weathering products (scorodite (78), goethite (9), red-blackish phases (14) and orange-reddish phases (14)). The specific number of analyses performed on each weathering phase is representative of the phase abundance. These analyses are indicated in Table 2 (only analyses given element contents for single phases were reflected, whereas those indicating phase mixture or presence of arsenopyrite were omitted). The scorodite chemical composition varies within short ranges, namely $Fe_2O_3$ = 34.0–37.8% and $As_2O_5$ = 46.4–51.2%, displaying really minor or trace concentrations of other elements (S, Ba, Cu and Al). This scorodite shows Fe/As molar ratios in the range 0.99–1.09, values very close to the theoretical value, with all the variations accounting for less than 10% as compared to the ideal value. The corresponding electron backscatter images reveal the important occurrence of colloform scorodite (Fig. 3e). The chemical composition of the orange-reddish phases is very variable, without clear stoichiometry, showing $Fe_2O_3$ and $As_2O_5$ contents in the ranges 30.7–49.1% and 25.3–42.1%, respectively. Their $SO_3$ content is relatively low, ranging from 0.04 to 3.84%. Occasionally some impurities of Cu, K, Ba and, in a lesser extent, Zn and Ca are present. The described chemical composition of these amorphous gels with the typical mudcrack-type texture, also observed in the electron backscatter images (Fig. 3f), confirms that these are constituted by AFA. The presence of amorphous ferric sulphoarsenates (AISA) can be discarded in view of their low $SO_3$ content. The Fe/As molar ratios of these compounds vary from 1.21 to 2.51.

The analyses carried out on goethite show $Fe_2O_3$ and $As_2O_5$ contents comprised, respectively, in the ranges 59.0–79.1% and 0.32–1.38%. The indicated $As_2O_5$ values agree well with the As(V) adsorption capacities reported in literature for this mineral [27,28]. Significant $SiO_2$ contents are also displayed by this mineral, from 0.56 to 9.43%, with the highest values in correspondence to the lowest $Fe_2O_3$ contents. The chemical composition of the other red-blackish phases displays $Fe_2O_3$ and $As_2O_5$ contents comprised, respectively, in the ranges 50.1–63.3% and 16.4–21.7%. Such high

**Table 2**
Chemical analyses of the arsenopyrite weathering products in the Terrubias mine wastes (Sc: scorodite and Gth: goethite).

| Phases | $Fe_2O_3$ (%) | $As_2O_5$ (%) | $SO_3$ (%) | $Al_2O_3$ (%) | $SiO_2$ (%) | CuO (%) | $K_2O$ (%) | BaO (%) | ZnO (%) | CaO (%) |
|---|---|---|---|---|---|---|---|---|---|---|
| Sc | 37.0 | 49.2 | 0.20 | n.d. | n.d. | 0.16 | n.d. | n.d. | n.d. | n.d. |
| Sc | 34.0 | 49.4 | 0.04 | n.d. | n.d. | n.d. | n.d. | n.d. | n.d. | n.d. |
| Sc | 35.5 | 51.2 | n.d. | n.d. | n.d. | n.d. | n.d. | n.d. | n.d. | n.d. |
| Sc | 37.5 | 49.5 | 0.12 | n.d. | n.d. | n.d. | n.d. | n.d. | n.d. | n.d. |
| Sc | 36.1 | 49.5 | 0.31 | n.d. | n.d. | 0.12 | n.d. | 0.04 | n.d. | n.d. |
| Sc | 35.8 | 49.2 | 0.12 | n.d. | n.d. | 0.28 | n.d. | 0.09 | n.d. | n.d. |
| Sc | 35.9 | 49.6 | 0.12 | n.d. | n.d. | 0.11 | n.d. | n.d. | n.d. | n.d. |
| Sc | 36.2 | 50.0 | 0.26 | n.d. | n.d. | 0.23 | n.d. | n.d. | n.d. | n.d. |
| Sc | 37.8 | 49.1 | 0.08 | n.d. | n.d. | n.d. | n.d. | n.d. | n.d. | n.d. |
| Sc | 36.8 | 49.7 | 0.10 | n.d. | n.d. | n.d. | n.d. | n.d. | n.d. | n.d. |
| Sc | 35.5 | 49.7 | 0.20 | 0.12 | n.d. | n.d. | n.d. | n.d. | n.d. | n.d. |
| Sc | 35.1 | 47.1 | 0.34 | 0.20 | n.d. | n.d. | n.d. | n.d. | n.d. | n.d. |
| Sc | 36.0 | 49.4 | 0.14 | n.d. | n.d. | n.d. | n.d. | n.d. | n.d. | n.d. |
| Sc | 37.2 | 49.8 | 0.08 | n.d. | n.d. | n.d. | n.d. | n.d. | n.d. | n.d. |
| Sc | 36.9 | 50.0 | 0.19 | n.d. | n.d. | n.d. | n.d. | n.d. | n.d. | n.d. |
| Sc | 37.2 | 49.6 | 0.34 | n.d. | n.d. | n.d. | n.d. | n.d. | n.d. | n.d. |
| Sc | 36.8 | 49.7 | 0.28 | n.d. | n.d. | n.d. | n.d. | n.d. | n.d. | n.d. |
| Sc | 36.5 | 49.3 | 0.24 | n.d. | n.d. | n.d. | n.d. | n.d. | n.d. | n.d. |
| Sc | 36.3 | 49.2 | 0.24 | n.d. | n.d. | n.d. | n.d. | n.d. | n.d. | n.d. |
| Sc | 34.9 | 48.8 | 0.25 | n.d. | n.d. | n.d. | n.d. | n.d. | n.d. | n.d. |
| Sc | 36.9 | 50.4 | 0.23 | n.d. | n.d. | n.d. | n.d. | n.d. | n.d. | n.d. |
| Sc | 36.9 | 49.9 | 0.22 | n.d. | n.d. | n.d. | n.d. | n.d. | n.d. | n.d. |
| Sc | 37.5 | 49.5 | 0.29 | n.d. | n.d. | n.d. | n.d. | n.d. | n.d. | n.d. |
| Sc | 36.6 | 46.4 | 0.63 | n.d. | n.d. | n.d. | n.d. | n.d. | n.d. | n.d. |
| Sc | 36.9 | 50.9 | 0.11 | n.d. | n.d. | n.d. | n.d. | n.d. | n.d. | n.d. |
| Sc | 37.0 | 50.0 | 0.16 | 0.12 | n.d. | n.d. | n.d. | n.d. | n.d. | n.d. |
| Sc | 37.2 | 49.8 | 0.20 | n.d. | n.d. | n.d. | n.d. | n.d. | n.d. | n.d. |
| AFA | 40.4 | 39.0 | 2.14 | n.d. | n.d. | 0.98 | 0.23 | 0.19 | n.d. | n.d. |
| AFA | 37.1 | 25.3 | 3.07 | n.d. | n.d. | 0.33 | n.d. | n.d. | n.d. | n.d. |
| AFA | 50.2 | 28.7 | 0.36 | n.d. | n.d. | n.d. | n.d. | n.d. | n.d. | n.d. |
| AFA | 33.2 | 28.1 | 0.18 | n.d. | n.d. | n.d. | n.d. | n.d. | 0.22 | n.d. |
| AFA | 49.1 | 31.3 | 0.42 | n.d. | n.d. | n.d. | n.d. | n.d. | n.d. | 0.10 |
| AFA | 49.0 | 31.2 | 0.40 | n.d. | n.d. | n.d. | n.d. | n.d. | n.d. | n.d. |
| AFA | 37.3 | 39.1 | 0.04 | n.d. | n.d. | n.d. | 2.42 | 0.20 | n.d. | n.d. |
| AFA | 36.3 | 37.3 | 2.28 | n.d. | n.d. | n.d. | 0.67 | 4.10 | n.d. | n.d. |
| AFA | 43.5 | 42.1 | 0.33 | n.d. | n.d. | 0.37 | n.d. | n.d. | n.d. | n.d. |
| AFA | 43.2 | 41.2 | 0.47 | n.d. | n.d. | 0.11 | n.d. | n.d. | n.d. | 0.10 |
| AFA | 30.7 | 33.7 | 1.47 | n.d. | n.d. | n.d. | n.d. | n.d. | n.d. | n.d. |
| AFA | 31.1 | 37.0 | 1.27 | n.d. | n.d. | n.d. | n.d. | n.d. | n.d. | n.d. |
| AFA | 36.4 | 34.2 | 3.84 | n.d. | n.d. | n.d. | n.d. | n.d. | n.d. | n.d. |
| AFA | 39.9 | 35.4 | 3.73 | n.d. | n.d. | n.d. | n.d. | n.d. | n.d. | n.d. |
| Gth | 59.0 | 0.38 | n.d. | n.d. | 9.43 | n.d. | n.d. | n.d. | n.d. | n.d. |
| Gth | 65.6 | 0.32 | n.d. | n.d. | 6.08 | n.d. | n.d. | n.d. | n.d. | n.d. |
| Gth | 66.2 | 0.73 | n.d. | n.d. | 5.86 | n.d. | n.d. | n.d. | n.d. | n.d. |
| Gth | 75.1 | 0.51 | n.d. | n.d. | 1.65 | n.d. | n.d. | n.d. | n.d. | n.d. |
| Gth | 68.3 | 0.70 | n.d. | n.d. | 2.21 | n.d. | n.d. | n.d. | n.d. | n.d. |
| Gth | 77.3 | 0.86 | n.d. | n.d. | 0.99 | n.d. | n.d. | n.d. | n.d. | n.d. |
| Gth | 79.1 | 1.38 | n.d. | n.d. | 0.69 | n.d. | n.d. | n.d. | n.d. | n.d. |
| Gth | 74.3 | 0.91 | n.d. | n.d. | 0.77 | n.d. | n.d. | n.d. | n.d. | n.d. |
| Gth | 73.2 | 0.92 | n.d. | n.d. | 0.56 | n.d. | n.d. | n.d. | n.d. | n.d. |
| HFO | 62.2 | 18.1 | 1.41 | n.d. | n.d. | 0.29 | n.d. | 0.13 | n.d. | n.d. |
| HFO | 51.7 | 18.7 | 1.80 | n.d. | n.d. | 0.10 | n.d. | n.d. | n.d. | 0.20 |
| HFO | 50.1 | 16.7 | 1.08 | n.d. | n.d. | 0.11 | n.d. | n.d. | n.d. | 0.10 |
| HFO | 61.3 | 21.7 | 0.59 | n.d | n.d | 0.36 | n.d | n.d | n.d | 0.10 |
| HFO | 63.3 | 16.4 | 0.45 | n.d. | 1.56 | 0.45 | n.d. | n.d. | n.d. | 0.10 |

$As_2O_5$ values together with the apparent hydrous character of these phases (as derived from the low total elemental composition) suggest that these are constituted by HFO on which As(V) is adsorbed.

### 3.2.4. MicroRaman spectroscopy

Of the different weathering phases distinguished by polarizing microscopy (scorodite, goethite, red-blackish phases and orange-reddish phases) the corresponding microRaman spectra confirm the presence of scorodite and goethite. The representative micro-Raman spectrum of the analysed scorodite (Fig. 5c) displays the typical bands in the arsenate stretching (809 and 891 $cm^{-1}$) and low wavelength (337, 385, 420, 451 and 486 $cm^{-1}$) regions of scorodite. The Raman modes reflected by the representative spectrum of the analysed goethite (Fig. 5d) (240, 294, 383, 479 and 552 $cm^{-1}$) also correspond to the characteristic bands of pure goethite. The micro-analyses performed on the red-blackish and orange-reddish phases give spectra with no apparent Raman modes, confirming their low-crystalline or amorphous nature, as is the case of HFO and AFA, with which are, respectively, compatible.

### 3.2.5. Mössbauer spectroscopy

The Mössbauer spectra of the yellow-greenish and orange-reddish phases distinguished on the waste rocks collected from the mine dumps are indicated in Fig. 6c and d, respectively. The representative spectrum of the yellow-greenish phases is a superposition of two doublets, one of them really weak and with a very low contribution. The main doublet has values of $\delta = 0.40\ mm\ s^{-1}$ and $QS = 0.43\ mm\ s^{-1}$, compatible with those of scorodite. The representative spectrum of the orange-reddish phases is fitted by a sextet with $B_{HF} = 37T$, corresponding to that of goethite.

**Table 3**
Environmental characterisation of the Barruecopardo and Terrubias mine wastes.

| | | Barruecopardo | Terrubias |
|---|---|---|---|
| NNP (kg $CaCO_3$ $t^{-1}$) | | −60 | −350 |
| pH | | 1.82 | 1.82 |
| TCLP concentrations (mg $L^{-1}$) | As | 3.67 | 12.9 |
| | Cu | 0.008 | 0.319 |
| | Pb | 0.056 | 0.671 |
| | Zn | 0.013 | 0.743 |
| | Cd | 0.011 | 0.049 |
| Bioavailable fraction (mg $kg^{-1}$) $(NH_4)_2SO_4$ procedure | As | 76.4 | 52.1 |
| Bioavailable fraction (mg $kg^{-1}$) EDTA procedure | Cu | 0.608 | 12.9 |
| | Pb | 33.0 | 65.9 |
| | Zn | 0.328 | 12.6 |
| | Cd | <0.05 | 0.288 |

TCLP limits for toxic characterisation: As (5 mg $L^{-1}$), Cd (1 mg $L^{-1}$) and Pb (5 mg $L^{-1}$).

### 3.3. Environmental risk assessment of the arsenopyrite-bearing mine wastes

The environmental characterisation performed on the Barruecopardo and Terrubias mine wastes is reflected in Table 3. Mine wastes exhibit negative NNP. Theoretically, wastes with positive NNP values have no potential for acidification whereas wastes with negative NNP values do, especially at levels < - 30 kg $CaCO_3$ $t^{-1}$. Significant lower values are displayed by concerned mine wastes, indicating their potential of acid generation. Accordingly, the corresponding pH values are low. These pH values are also consistent with the occurrence and persistence of scorodite as main arsenopyrite weathering product. According to the TCLP test, the Terrubias mine wastes are characterised as toxic as the regulatory limits are greatly exceeded for As. The As leached from the Barruecopardo mine wastes also displays a concentration close to the limit for this characterisation. The bioavailable fraction of As as determined by the $(NH_4)_2SO_4$ extraction procedure shows important contents, reflecting higher values for wastes from the Barruecopardo mine. These concentrations could imply an As transference to different environmental compartments. In this regard, soil total concentrations of As about 1200 and 1350 mg $kg^{-1}$ have been reported in the environs of the Barruecopardo and Terrubias mine dumps, respectively [27]. The bioavailable fraction of the other toxic elements as determined by the EDTA extraction procedure displays in general relatively low contents, especially in wastes from the Barruecopardo mine, with Pb showing in both cases the highest values.

The parameters analysed to establish the water quality of the nearby ponds are indicated in Table 4. Lower pH and higher Eh values as well as lower concentrations of As and other toxic elements were shown by the pond present in the Barruecopardo mining area. The unexpected water characteristics found in the Terrubias mining area pond could be explained taking into account that carbonate and calcosilicate rocks outcrop in the basin of this pond. This feature minimises importantly the impact of mine wastes on water, raising water pH and decreasing the sulphate content as well as those of toxic elements existing as cationic species due to the formation of insoluble compounds.

**Table 4**
Water quality parameters of ponds present in the Barruecopardo and Terrubias mining areas.

| | Barruecopardo | Terrubias |
|---|---|---|
| pH | 3.45 | 7.81 |
| Eh (mV) | 518 | 142 |
| Sulphate (mg $L^{-1}$) | 600 | 185 |
| As (mg $L^{-1}$) | 0.218 | 0.133 |
| Cu (mg $L^{-1}$) | 0.444 | <0.005 |
| Pb (mg $L^{-1}$) | <0.05 | <0.05 |
| Zn (mg $L^{-1}$) | 1.86 | <0.005 |
| Cd (mg $L^{-1}$) | 0.009 | <0.005 |

P-rich scorodite, pharmacosiderite, goethite and HFO were the secondary products identified in the weathered arsenopyrite-rich wastes from the Barruecopardo mine, whereas scorodite, AFA, goethite and HFO were the weathering phases detected in wastes from the Terrubias mine. Such specific secondary phases are responsible for the As control in the studied mining areas.

In both of the studied mine wastes scorodite was found the most abundant oxidation product. Its formation takes place according to the following reaction [38]:

$$FeAsS + 14Fe^{3+} + 10H_2O \rightarrow 14Fe^{2+} + SO_4^{2-} + FeAsO_4 \cdot 2H_2O + 16H^+ \quad (1)$$

Many studies have been performed studying the solubility and stability of scorodite [38–41] and, although some discrepancy has been found between the reported solubility products ($K_s$: $10^{-21.7}$ to $10^{-25.4}$), scorodite is considered to have low solubility and relatively high stability under oxidising conditions. The solubility of scorodite is minimum (<0.5 mg As $L^{-1}$) at pH slightly less than 3, from which its incongruent dissolution takes place with the concomitant precipitation of HFO and As release according to the following reactions [42]:

$$FeAsO_4 \cdot 2H_2O + H_2O \rightarrow H_2AsO_4^- + Fe(OH)_3 + H^+ \quad (2)$$

$$FeAsO_4 \cdot 2H_2O + H_2O \rightarrow HAsO_4^{2-} + Fe(OH)_3 + 2H^+ \quad (3)$$

The released As is adsorbed on the precipitated HFO. These processes keep soluble As at really low levels up to pH values about 6 [39,40]. The scorodite solubility has been reported not to be influenced by the mineral particle size [43]. Moreover, its dissolution kinetic has been proven to be slow, with dissolution rates on the order of $10^{-10}$ to $10^{-11}$ mol $m^{-2}$ $s^{-1}$ [43,44], which explains why scorodite persists at mine waste sites after many years of weathering. Therefore, the prevalence of scorodite in the studied mine wastes should limit greatly the release of As into the surrounding environmental compartments, unless drastic condition changes (mainly redox and pH changes) take place. Anyway, it must be taken into account that phosphoscorodite is the mineral variety present in the Barruecopardo mine wastes, which could entail a differential behaviour. Thus, although considerable lower solubility values have been reported for strengite [45], it has been found that the presence of phosphate leads to the formation of P-rich scorodite of somewhat reduced stability [46]. This aspect together with the simultaneous incorporation of phosphate during the scorodite crystal lattice formation or the latter phosphate substitution for arsenate implies a reduced scavenger action of this mineral in the Barruecopardo mining area.

Low solubility values have been also reported for HFO and goethite, with $K_s$ values of $10^{-37.1}$ and $10^{-44.2}$, respectively [47]. In spite of the low solubility of HFO, their conversion to goethite can occur spontaneously in acidic media (also in basic media) through reconstructive transformation. However, high loads of As on HFO inhibit the transformation of these to the crystalline goethite [48]. This has important environmental implications since such decomposition proceeds with a release of As. Moreover, when goethite dominates the stability field of scorodite is significantly smaller than when HFO are the dominant species [44]. In this regard, the As loads shown by the HFO present in the Barruecopardo mine wastes are lower than those of the Terrubias mine, which may suppose a reduced inhibition of the HFO transformation to goethite, and so higher environmental risks. It is worth mentioning that, although goethite was found in mine wastes from both areas, in the case of

Barruecopardo mine wastes HFO and goethite are present as a continuous mixture, whereas in the Terrubias mine wastes HFO and goethite are mainly present as differentiated phases, with goethite only appearing very locally.

Concerning AFA, these have been proven to display higher solubilities ($K_s$: $10^{-23.0}$) and dissolution rates than scorodite, about 100 times higher [2,40,43,49]. AFA show low stability, dissolving incongruently from a lower pH value than scorodite [43]. These compounds are considered the precursors to scorodite formation, being a dissolution process suggested as the mechanism involved in this transformation [50]. AFA were only detected in the Terrubias mining area, showing a really restricted presence, which is consistent with the mentioned characteristics and transformation. Such conversion should limit the As dispersion into the environment.

To our knowledge, no solubility and thermodynamic data have been determined for pharmacosiderite, so its role in the As control in the Barruecopardo mine wastes in which this mineral appears cannot be assessed.

In general, it seems that the secondary products present in the studied mining areas should restrict importantly the As release from mine wastes provided that environmental conditions keep more or less stable. This aspect is especially important for scorodite (the most abundant arsenopyrite weathering product). The low pH displayed by mine wastes is responsible for the stability and low solubility of this mineral, and so for the derived As immobilisation. This low pH should be also determinant for the presence and stability of AFA. Anyway, in the case of Barruecopardo the P-rich environment and the relatively reduced As load shown by the HFO there present could enhance the As mobility and migration.

## 4. Conclusions

The long-term weathering of arsenopyrite-rich wastes from tungsten and tin mines, particularly from the abandoned exploitations of Barruecopardo and Terrubias (Spain), has generated diverse secondary As products, namely scorodite, pharmacosiderite and AFA with Fe/As molar ratios ranging from 1.2 to 2.5. Scorodite was found to prevail in both studied mining areas. This mineral occurs in variable particle sizes and textures and with different chemical composition depending on the original surrounding rock mineralogy. Thus, phosphoscorodite was the mineral variety detected in apatite-containing geoenvirons, with P contents up to 9% $P_2O_5$. Goethite and HFO were also identified as weathering phases, showing, respectively, As loads up to 1.4 and 22% $As_2O_5$. The characteristics and contents of all these secondary phases, i.e. low solubility of scorodite, low content of AFA and high capacity of HFO to adsorb As, should limit importantly the As release from these arsenopyrite-bearing wastes. Although in the case of wastes generated from P-rich geoenvirons and where the generated HFO display relatively reduced As loads (as happens in the Barruecopardo mining area) the As mobility and migration could be enhanced. Anyway, the environmental characterisation of these wastes reveals their toxic or hazardous character in terms of the TCLP test, the bioavailable fraction of As and the acid generation capacity. Therefore, proper planning should be undertaken to manage these wastes.

## Acknowledgments

This study was carried out under the projects SA091A08 funded by the "Junta de Castilla y León" and CGL2008-06357 funded by the Ministry of Science and Innovation of Spain.

## References

[1] B.J. Alloway, Heavy Metals in Soils, Blackie Academic & Professional, Glasgow, 1995.
[2] P. Drahota, M. Filippi, Secondary arsenic minerals in the environment: a review, Environ. Int. 35 (2009) 1243–1255.
[3] G.S. Pokrovski, S. Kara, J. Roux, Stability and solubility of arsenopyrite, FeAsS, in crustal fluids, Geochim. Cosmochim. Acta 66 (2002) 2361–2378.
[4] D. Craw, D. Falconer, J.H. Youngson, Environmental arsenopyrite stability and dissolution: theory, experiment, and field observations, Chem. Geol. 199 (2003) 71–82.
[5] C.L. Corkhill, D.J. Vaughan, Arsenopyrite oxidation—a review, Appl. Geochem. 24 (2009) 2342–2361.
[6] R.J. King, Minerals explained 35: arsenopyrite, Geol. Today 18 (2002) 72–75.
[7] M. Filippi, V. Goliáš, Z. Pertold, Arsenic in contaminated soils and anthropogenic deposits at the Mokrsko, Roudný, and Kašperské Hory gold deposits, Bohemian Massif (CZ), Environ. Geol. 45 (2004) 716–730.
[8] D. Paktunc, A. Foster, S. Heald, G. Laflamme, Speciation and characterization of arsenic in gold ores and cyanidation tailings using X-ray absorption spectroscopy, Geochim. Cosmochim. Acta 68 (2004) 969–983.
[9] R.L. Flemming, K.A. Salzsauler, B.L. Sherriff, N.V. Sidenko, Identification of scorodite in fine-grained, high-sulfide, arsenopyrite mine-waste using micro X-ray diffraction (μXRD), Can. Mineral. 43 (2005) 1243–1254.
[10] D. Mains, D. Craw, Composition and mineralogy of historic gold processing residues, east Otago, New Zealand, New Zeal. J. Geol. Geop. 48 (2005) 641–647.
[11] K.A. Salzsauler, N.V. Sidenko, B.L. Sherriff, Arsenic mobility in alteration products of sulfide-rich, arsenopyrite-bearing mine wastes, Snow Lake, Manitoba, Canada, Appl. Geochem. 20 (2005) 2303–2314.
[12] M.F. Lengke, C. Sanpawanitchakit, R.N. Tempel, The oxidation and dissolution of arsenic-bearing sulfides, Can. Mineral. 47 (2009) 593–613.
[13] H.W. Nesbitt, I.J. Muir, Oxidation states and speciation of secondary products on pyrite and arsenopyrite reacted with mine waste and waters and air, Miner. Petrol. 62 (1998) 123–144.
[14] R. Gieré, N.V. Sidenko, E.V. Lazareva, The role of secondary minerals in controlling the migration of arsenic and metals from high-sulfide wastes (Berikul gold mine, Siberia), Appl. Geochem. 18 (2003) 1347–1359.
[15] S.R. Walker, H.E. Jamieson, A. Lanzirotti, C.F. Andrade, G.E.M. Hall, The speciation of arsenic in iron oxides in mine wastes from the giant gold mine, N.W.T.: application of synchrotron micro-XRD and micro-xanes at the grain scale, Can. Mineral. 43 (2005) 1205–1224.
[16] S.R. Walker, M.B. Parsons, H.E. Jamieson, A. Lanzirotti, Arsenic mineralogy of near-surface tailings and soils: Influences on arsenic mobility and bioaccessibility in the nova scotia gold mining districts, Can. Mineral. 47 (2009) 533–556.
[17] L. Haffert, D. Craw, Mineralogical controls on environmental mobility of arsenic from historic mine processing residues, New Zealand, Appl. Geochem. 23 (2008) 1467–1483.
[18] P.-K. Lee, M.-J. Kang, S.-H. Choi, J.-C. Touray, Sulfide oxidation and the natural attenuation of arsenic and trace metals in the waste rocks of the abandoned Seobo tungsten mine, Korea, Appl. Geochem. 20 (2005) 1687–1703.
[19] M.E.P. Gomes, P.J.C. Favas, Mineralogical controls on mine drainage of the abandoned Ervedosa tin mine in north-eastern Portugal, Appl. Geochem. 21 (2006) 1322–1334.
[20] B.M. Petrunic, T.A. Al, L. Weaver, A transmission electron microscopy analysis of secondary minerals formed in tungsten-mine tailings with an emphasis on arsenopyrite oxidation, Appl. Geochem. 21 (2006) 1259–1273.
[21] E. Pellitero, Geologic and genetic factors in the tungsten-deposits of the north of the Salamanca province, Cuadernos do Laboratorio Xeolóxico de Laxe 2 (1981) 245–257 (in Spanish).
[22] E. Pellitero, The tungsten central-eastern region of Salamanca, Cuadernos do Laboratorio Xeolóxico de Laxe 2 (1981) 227–244 (in Spanish).
[23] A.A. Sobek, W.A. Schuller, J.R. Freeman, R.M. Smith, Field and laboratory methods applicable to overburden and minesoils, U.S EPA (EPA 600/2-78-054), Cincinnati, Ohio, 1978.
[24] W.W. Wenzel, N. Kirchbaumer, T. Prohaska, G. Stingeder, E. Lombi, D.C. Adriano, Arsenic fractionation in soils using an improved sequential extraction procedure, Anal. Chim. Acta 436 (2001) 309–323.
[25] A. Kontopoulos, K. Komnitsas, A. Xenidis, N. Papassiopi, Environmental characterisation of the sulphidic tailings in Lavrion, Miner. Eng. 8 (1995) 1209–1219.
[26] S. Endo, Y. Terada, Y. Kato, I. Nakai, Chemical speciation of arsenic-accumulating mineral in a sedimentary iron deposit by synchrotron radiation multiple X-ray analytical techniques, Environ. Sci. Technol. 42 (2008) 7152–7158.
[27] A. Garcia-Sanchez, E. Alvarez-Ayuso, F. Rodriguez-Martin, Sorption of As(V) by some oxyhydroxides and clay minerals. Application to its immobilization in two polluted mining soils, Clay Miner. 37 (2002) 187–194.
[28] P. Lakshmipathiraj, B.R.V. Narasimhan, S. Prabhakar, G. Bhaskar Raju, Adsorption of arsenate on synthetic goethite from aqueous solutions, J. Hazard. Mater. 136 (2006) 281–287.
[29] M.L. Pierce, C.B. Moore, Adsorption of arsenite and arsenate on amorphous iron hydroxide, Water Res. 16 (1982) 1247–1253.
[30] B.A. Manning, S. Goldberg, Modeling competitive adsorption of arsenate with phosphate and molybdate on oxide minerals, Soil Sci. Soc. Am. J. 60 (1996) 121–131.
[31] E.E. Coleyshaw, W.P. Griffith, R.J. Bowell, Fourier-transform Raman spectroscopy of minerals, Spectrochim. Acta Part A: Mol. Spectrosc. 50 (1994) 1909–1918.
[32] M. Filippi, V. Machovič, P. Drahota, V. Böhmová, Raman microspectroscopy as a valuable additional method to X-ray diffraction and electron microscope/microprobe analysis in the study of iron arsenates in environmental samples, Appl. Spectrosc. 63 (2009) 621–626.

[33] M.A. Gomez, H. Assaaoudi, L. Becze, J.N. Cutler, G.P. Demopoulos, Vibrational spectroscopy study of hydrothermally produced scorodite ($FeAsO_4{\cdot}2H_2O$), ferric arsenate sub-hydrate (FAsH; $FeAsO_4{\cdot}0.75H_2O$) and basic ferric arsenate sulfate (BFAS; $Fe[(AsO_4)_{1-x}(SO_4)_x(OH)_x]{\cdot}wH_2O$), J. Raman Spectrosc. 41 (2010) 212–221.
[34] D.L.A. de Faria, S. Venâncio Silva, M.T. de Oliveira, Raman microspectroscopy of some iron oxides and oxyhydroxides, J. Raman Spectrosc. 28 (1997) 873–878.
[35] M. Takano, T. Takada, T. Wada, K. Okada, Magnetic properties of $FeAsO_4{\cdot}2H_2O$ and $KFe_4(OH)_4(AsO_4)_3{\cdot}8H_2O$, J. Phys. Soc. Jpn. 31 (1971) 298.
[36] R.E. Vandenberghe, E. De Grave, C. Landuydt, L.H. Bowen, Some aspects concerning the characterization of iron oxides and hydroxides in soils and clays, Hyp. Interact. 53 (1990) 175–196.
[37] T.S. Berquó, R.A.L. Imbernon, A. Blot, D.R. Franco, M.C.M. Toledo, C.S.M. Partiti, Low temperature magnetism and Mössbauer spectroscopy study from natural goethite, Phys. Chem. Miner. 34 (2007) 287–294.
[38] P.M. Dove, J.A. Rimstidt, The solubility and stability of scorodite, $FeAsO_4{\cdot}2H_2O$, Am. Mineral. 70 (1985) 838–844.
[39] E. Krause, V.A. Ettel, Solubilities and stabilities of ferric arsenate compounds, Hydrometallurgy 22 (1989) 311–337.
[40] D. Langmuir, J. Mahoney, J. Rowson, Solubility products of amorphous ferric arsenate and crystalline scorodite ($FeAsO_4{\cdot}2H_2O$) and their application to arsenic behavior in buried mine tailings, Geochim. Cosmochim. Acta 70 (2006) 2942–2956.
[41] M.C. Bluteau, G.P. Demopoulos, The incongruent dissolution of scorodite – solubility, kinetics and mechanism, Hydrometallurgy 87 (2007) 163–177.
[42] D.K. Nordstrom, D.G. Archer, Arsenic thermodynamic data and environmental geochemistry, in: A.H. Welch, K.G. Stollenwerk (Eds.), Arsenic in Ground Water, Kluwer Academic Publishers, Boston, Massachusetts, USA, 2003.
[43] D. Paktunc, K. Bruggeman, Solubility of nanocrystalline scorodite and amorphous ferric arsenate: implications for stabilization of arsenic in mine wastes, Appl. Geochem. 25 (2010) 674–683.
[44] M.C. Harvey, M.E. Schreiber, J.D. Rimstidt, M.M. Griffith, Scorodite dissolution kinetics: implications for arsenic release, Environ. Sci. Technol. 40 (2006) 6709–6714.
[45] M. Iuliano, L. Ciavatta, G. De Tommaso, On the solubility constant of strengite, Soil Sci. Soc. Am. J. 71 (2007) 1137–1140.
[46] S. Singhania, Q. Wang, D. Filippou, G.P. Demopoulos, Acidity, valency and third-ion effects on the precipitation of scorodite from mixed sulfate solutions under atmospheric-pressure conditions, Metall. Mater. Trans. B: Process Metall. Mater. Process. Sci. 37 (2006) 189–197.
[47] D.O Whittemore, D. Langmuir, Ferric oxyhydroxide microparticles in water, Environ. Health Persp. 9 (1974) 173–176.
[48] R.G. Ford, Rates of hydrous ferric oxide crystallization and the influence on coprecipitated arsenate, Environ. Sci. Technol. 36 (2002) 2459–2463.
[49] N.J. Welham, K.A. Malatt, S. Vukcevic, The stability of iron phases presently used for disposal from metallurgical systems—a review, Miner. Eng. 13 (2000) 911–931.
[50] D. Paktunc, J. Dutrizac, V. Gertsman, Synthesis and phase transformations involving scorodite, ferric arsenate and arsenical ferrihydrite: Implications for arsenic mobility, Geochim. Cosmochim. Acta 72 (2008) 2649–2672.